Influence of hydrothermal powder morphology on the sintered microstructure of MnZn ferrites

Anderson Dias,[a] Roberto M. Paniago[b] and Vicente T. L. Buono[a]

[a]*Departamento de Engenharia Metalúrgica e de Materiais, EE-UFMG, Rua Espírito Santo, 35/Sala 206, 30160–030, Belo Horizonte, MG, Brazil*

[b]*Departamento de Física, ICEx-UFMG, CP702, 30123–970, Belo Horizonte, MG, Brazil*

The influence of hydrothermal powder morphology on the sintered microstructure of MnZn ferrites has been analysed. Changes in lattice parameter, particle size, density, size and total volume of pores and in the surface area of the particles were studied as functions of hydrothermal temperature and time. The ferrites were sintered at 1250 °C in a dry nitrogen atmosphere. High density and surface homogeneous ceramic bodies were obtained, without zinc loss by volatilisation. It has been observed that small differences on the properties of the hydrothermal powders gave rise to rather different microstructures after sintering. The effects of the surface chemistry of the nanosized ferrite particles and of the sintering atmosphere employed are discussed, in order to explain this behaviour. Finally, the magnetic character of the ferrite powders as well as of the sintered bodies was analysed at different conditions of temperature and applied magnetic field.

The interest in the wet-chemical synthesis of ultrafine ferrite powders enabling production of ceramics with high density at low temperatures is unquestionable. Hydrothermal processing meets the increasing demand for the preparation of these powders. As an alternative or new approach, hydrothermal synthesis is less energy consuming and less polluting than the other techniques of ceramic powder manufacture. Crystalline oxides of high quality have been prepared from natural sources or metallic powders at moderate temperatures and pressures.[1,2] The use of supercritical water as the reactant or phase separation medium has promoted the new field of sintering oxides at relatively low temperatures and preparation of novel carbons.[3] The application of the hydrothermal processing concepts can also be expanded to non-aqueous systems, as discussed by Kolb *et al.*[4] The major advantage of this process over conventional and other advanced processes is the possibility of preparing highly crystalline powders with controlled particle size and stoichiometry, eliminating the need for high-temperature calcination and subsequent milling.

This work employs the hydrothermal synthesis to produce soft magnetic MnZn ferrite powders with the required characteristics for direct pressing and sintering. These were attained for a set of processing conditions, by means of which crystalline, single-phase, impurity-free MnZn ferrite powders were obtained with narrow particle size distribution. The results reported here show that small differences in powder morphology and structure, owing to the use of different hydrothermal conditions, influence substantially the microstructure of the specimens after sintering. The surface chemistry of the nanosized particles and the magnetic behaviour of the ferrites are correlated to the morphological and microstructural properties.

Experimental

The powders investigated were produced by hydrothermal processing, in a stainless steel autoclave, of salts containing iron, manganese and zinc, as well as sodium hydroxide and hydrogen peroxide. Initially, the precursors were dissolved in deionized water and mixed, followed by addition of the oxidizer and precipitant agents. The volume of the resultant solution was always around 30% of the autoclave total volume. Conditions selected for this study involve synthesis at temperatures ranging from 110 to 190 °C for times between 4 h and 30 h, under saturated vapour pressure. The powders were washed using different quantities of water and ethanol, centrifuged (4000 rpm, 5 min) and dried at 60 °C. The stoichiometry obtained under these conditions was $Mn_{0.48}Zn_{0.52}Fe_2O_4$, as determined by atomic absorption spectroscopy, X-ray fluorescence (XRF) and energy-dispersive spectrometry (EDS). A sequential X-ray spectrometer fitted with a rhodium target end window X-ray tube and an analytical software were employed for the XRF analysis.

The Brunauer–Emmett–Teller (BET) technique was used to characterise the specific surface area, pore size distribution, mean size and total volume of pores. Prior to the analysis, the powders were degassed at 150 °C for 1 h. An X-ray diffractometer, operating with Cu-Kα radiation and equipped with a graphite crystal monochromator, was used to characterise the crystalline phases and to determine, from broadening of the diffraction lines (220), (333), (440) and (553), the average particle size.[5] Densities of the ferrite powders were determined by a helium pycnometer. From these results and those obtained by BET, the particle size was calculated.[6] The iron(II) ion concentration was determined through wet-chemical analysis according to the American Society for Testing and Materials (ASTM) D3852/1986–1991. Scanning electron microscopy (SEM) was employed to study the morphology of the ferrite powders.

Green ferrite ceramics were prepared using polyvinylalcohol as binder and cold pressed uniaxially at 490 MPa forming cylindrical specimens of 5 mm height and 25 mm diameter. A pre-sintering step at 600 °C for 2 h was employed, followed by sintering at 1250 °C for 15 h in a tubular furnace (± 1 °C), under constant heating/cooling rates (3 °C min^{-1}). The sintering atmosphere used was dry nitrogen (5 ppm water) and oxygen (10 ppm water) at flow rates of 3 and 30 ml min^{-1}, respectively. Chemical analysis was done in the ceramic bodies in order to find compositional variations, particularly zinc loss. Sintered bodies were fractured or cut using a diamond saw blade and polished with diamond paste. An HCl–HF (v/v = 3.1) solution was employed to enhance microstructural features of polished surfaces, which were then analysed by X-ray diffraction (XRD), SEM and EDS. True densities of the ceramic bodies were determined using a helium pycnometer.

Mössbauer spectroscopic studies were carried out using a

conventional constant acceleration spectrometer. The magnetic character of the hydrothermal powders and of the sintered bodies was evaluated at 77 and at 300 K with an applied magnetic field of 2 kG. The ferrite powders and the milled sintered ceramics were pressed with an acrylic resin, in order to form discs of 2 mm height and 12 mm diameter.

Results and Discussion

Fig. 1 shows a SEM image of the ferrite powder hydrothermally synthesised at 110 °C. Fig. 2(a) presents the XRD pattern of the ferrite shown in Fig. 1 and Fig. 2(b) that of the corresponding sintered ceramic body. As can be seen in Fig. 1, the crystalline ferrite powders are formed by weak agglomerates of nanoparticles, which could only be individually resolved through atomic force microscopy.[7] The XRD peaks of the spinel ferrites produced at different hydrothermal temperatures and times were essentially the same, except in half-peak width, a parameter strongly correlated to the crystallite size. We observe broad peaks for the hydrothermally produced MnZn ferrites; the crystallite size for all samples was calculated on the basis of the equation of Williamson–Hall.[5] As shown in Fig. 3, the particle sizes estimated from the XRD results are in good agreement with those obtained by BET and this result indicates that powder agglomeration was not significant. Often, these agglomerates are weakly bound by surface and capillary forces, either electrostatic or of the van der Waals type, and are easily destroyed by moderate external applied loads, for example during the compacting stage. Particle sizes measured on atomic force microscopy images taken at the surface of

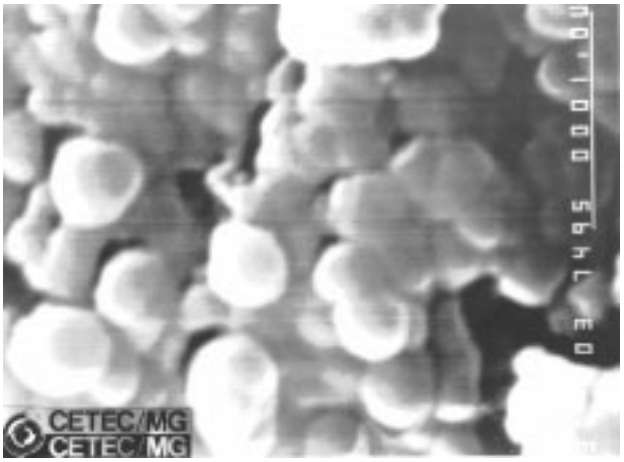

Fig. 1 SEM micrograph of the MnZn ferrite powder synthesised at 110 °C

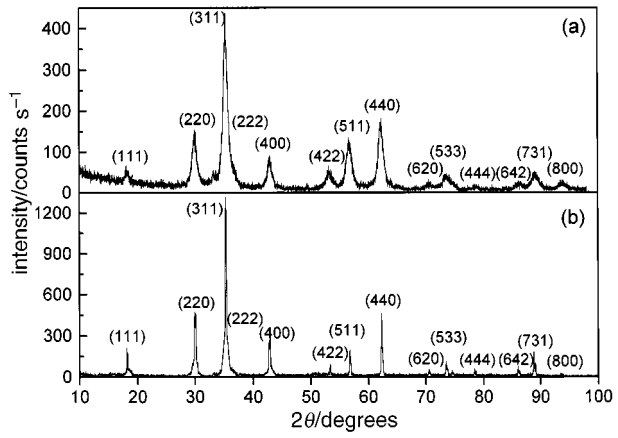

Fig. 2 XRD patterns of (a) the ferrite powder produced hydrothermally at 110 °C, and (b) the sintered ceramic

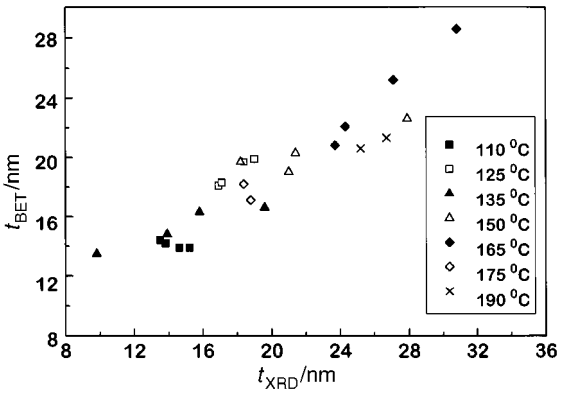

Fig. 3 Particle size calculated from X-ray line broadening (t_{XRD}) *vs.* particle size determined from BET measurements (t_{BET}). The temperatures employed in the hydrothermal synthesis are indicated.

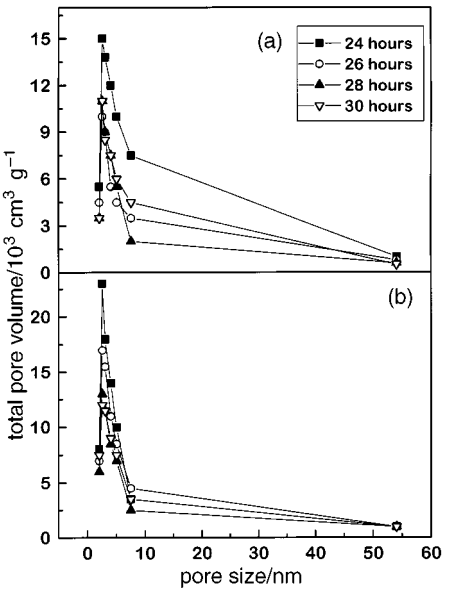

Fig. 4 Pore size distributions for the hydrothermal ferrite powders produced at 125 (a) and 110 °C (b)

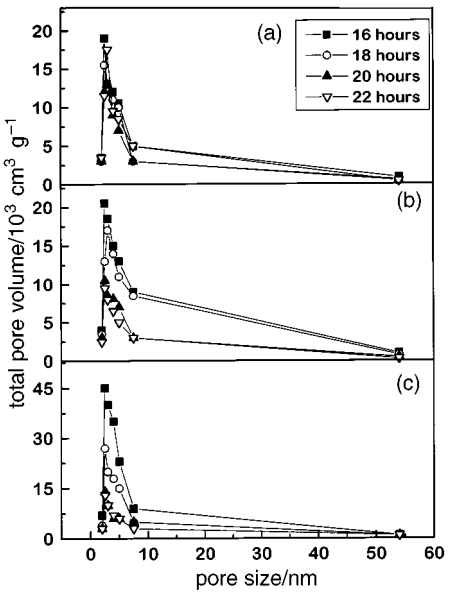

Fig. 5 Pore size distributions for the hydrothermal ferrite powders produced at 165 (a), 150 (b) and 135 °C (c)

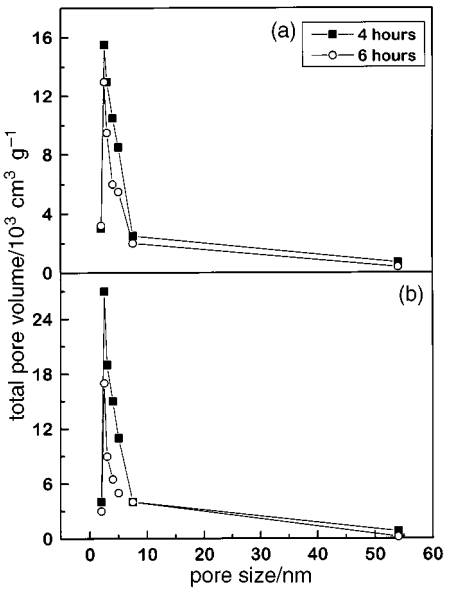

Fig. 6 Pore size distributions for the hydrothermal ferrite powders produced at 190 (a) and 175 °C (d)

pressed samples ranged from 10 to 40 nm[7] and are in good agreement with measurements made using XRD and BET.

The morphological parameters of the hydrothermal powders are presented in Table 1, which lists the values of specific surface area, pore size, density and lattice parameters of the MnZn ferrites for each processing temperature and time employed. Although the changes observed on these parameters are small (see the relative errors in Table 1), there is a strong tendency for higher processing temperatures to produce larger particles with smaller pores. Fig. 4–6 show the pore size distribution for all samples produced. The total volume of pores decreases with increasing processing temperature or time; consequently, denser powders are obtained (Table 1). The adsorption and desorption curves presented no hysteresis, indicating that the pores are cylindrical in shape.[6] Densities measured on sintered specimens show very little change with temperature of hydrothermal synthesis. The values obtained were between 4.89 and 5.03 g cm^{-3} and are close (94.8–97.5%) to the theoretical maximum density. These results are in accord with the observations of Komarneni *et al.*[8] and Dias *et al.*[9] concerning NiZn ferrites sintered from hydrothermal powders. According to Zhao and Harmer,[10,11] narrow particle size distribution and small pores can lead to final densities after sintering which are close to the theoretical density.

Fig. 7 shows micrographs obtained by SEM of sintered samples from the hydrothermal powders produced at 110, 135, 165 and 190 °C. We can see that the small differences observed on the properties of the synthesised powders (Table 1) gave rise to rather different microstructures after sintering. Specimens obtained from powders produced at higher temperatures have larger grains and less porosity (Fig. 7). Densification and grain growth of manganese zinc ferrites during sintering depend on a number of parameters, such as particle size, morphology, agglomeration state and impurity level.[9] The surface chemistry of nanosized ferrite particles is also important, because it governs the surface and grain boundary diffusion, dominant processes during sintering.[9] In addition, the surface chemistry can drastically influence powder agglomeration. For example, water-washed hydroxide precipitates, after the chemical preparation of ceramic powders, involve hydrogen bonding of surface hydroxy groups, leading to strong agglomeration,[12] which drastically influences sintering and microstructural evolution. However, during hydrothermal treatment of hydroxide suspension, the crystallisation of ferrite particles eliminates the hydroxy groups [eqn. (1)].

$$x\mathrm{Mn}^{+2}+y\mathrm{Zn}^{+2}+(3-x-y)\mathrm{Fe}^{+3}+8\mathrm{OH}^{-} \Rightarrow \mathrm{Mn}_x\mathrm{Zn}_y\mathrm{Fe}_{3-x-y}\mathrm{O}_4+4\mathrm{H}_2\mathrm{O}\ (x+y=1) \quad (1)$$

The extent of crystallisation, or the number of remaining hydroxy groups on the particle surface, depends on the synthesis temperature. Essentially, it is verified that the number of water molecules bound *via* hydrogen bonds on the particle surface diminishes as the synthesis temperature is increased. In the present work, denser powders were produced at higher processing temperatures, which accelerate the densification and grain growth kinetics. Consequently, ceramic bodies with increasing density and grain size were observed for increasing hydrothermal temperatures. As can be seen in Fig. 7, the grain size of the sintered ferrites varied from 2 ± 1 μm (for ceramics obtained from powders produced at 110 °C) to 45 ± 8 μm (for bodies sintered from ferrites synthesised at 190 °C).

The results of XRD for the sintered bodies showed only the

Table 1 Morphological characteristics of the hydrothermal ferrite powders for the various hydrothermal temperatures and times employed

temp./°C	time/h	surface area/m^2 g^{-1}	pore size/nm	density/g cm^{-3}	lattice parameter/nm
110	24	100.5±1.3	4.2±0.1	4.16±0.02	0.8453
110	26	99.9±1.1	4.0±0.1	4.24±0.02	0.8455
110	28	99.6±1.0	3.8±0.2	4.32±0.03	0.8459
110	30	99.2±1.0	3.8±0.1	4.35±0.03	0.8459
125	24	75.9±0.5	3.8±0.1	4.37±0.01	0.8454
125	26	74.3±0.3	3.8±0.1	4.42±0.03	0.8458
125	28	68.3±0.3	3.6±0.1	4.46±0.02	0.8462
125	30	66.5±0.4	3.4±0.1	4.54±0.03	0.8465
135	16	118.5±1.1	5.1±0.2	3.76±0.03	0.8438
135	18	96.6±1.2	3.7±0.2	4.19±0.04	0.8442
135	20	83.4±0.6	3.6±0.1	4.41±0.04	0.8454
135	22	80.5±0.5	3.2±0.1	4.50±0.03	0.8457
150	16	70.3±0.7	3.8±0.1	4.33±0.02	0.8451
150	18	68.7±0.5	3.6±0.1	4.60±0.04	0.8457
150	20	63.2±0.7	3.2±0.1	4.68±0.04	0.8461
150	22	55.8±0.8	3.0±0.1	4.75±0.05	0.8463
165	16	65.8±0.6	3.4±0.2	4.38±0.04	0.8455
165	18	57.6±0.7	3.3±0.1	4.72±0.03	0.8461
165	20	50.0±0.6	2.9±0.1	4.77±0.04	0.8464
165	22	43.2±0.5	2.9±0.1	4.85±0.03	0.8470
175	4	78.1±0.4	3.8±0.1	4.81±0.02	0.8444
175	6	76.6±0.6	3.5±0.1	4.57±0.01	0.8450
190	4	62.7±0.5	3.5±0.1	4.65±0.01	0.8455
190	6	60.0±0.3	3.1±0.1	4.70±0.03	0.8463

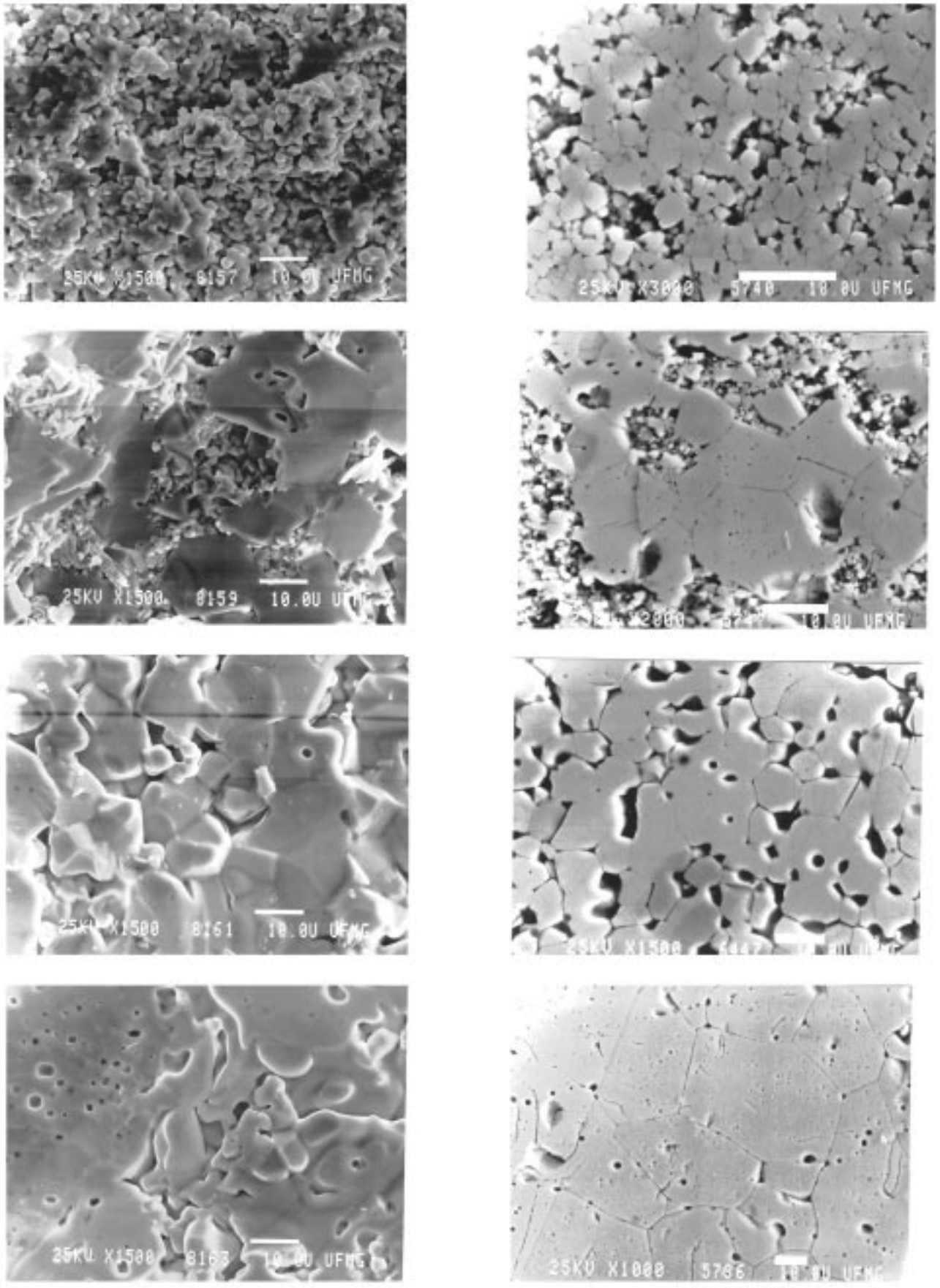

Fig. 7 MnZn ferrite microstructural evolution with hydrothermal synthesis temperature (from top to bottom: 110, 135, 165 and 190 °C), fractured (left) and polished (right) surfaces

presence of the spinel phase [Fig. 2(b)], which establishes the high quality of the sintering atmosphere used. It has been observed[13] that sintering atmospheres with high oxygen pressures can lead to formation of α-Fe_2O_3. The XRF spectra for MnZn ferrites produced at different hydrothermal temperatures and times were very similar to those obtained for the sintered ceramics. Fig. 8 presents the XRF spectra for a MnZn ferrite produced hydrothermally at 110 °C. The zinc concentration was carefully investigated in all ceramic powders and sintered bodies, in order to verify if zinc loss by volatilisation took place. Recently, Majima *et al.*[14,15] analysed the zinc-loss phenomenon in ferrites, and showed that zinc volatilisation leads to variations in the iron(II) ion concentration. Chemical analysis of the hydrothermal powders and sintered ceramics showed that the Fe^{2+} concentration has no variation between samples and the average value was 0.033%. Around ten regions of the powders, produced at different hydrothermal conditions of temperature and time, were also analysed by EDS. The results showed no relevant compositional variation, which indicates that the ceramics are chemically homogeneous.

The lattice parameter evolution in MnZn ferrites as a function of the temperature was studied by Majima *et al.*,[14,15] Zaharescu *et al.*[16] and Kimura and Chiba.[17] They found smaller values in powders obtained at lower temperatures of treatment. These observed values were close to that of the zinc ferrite, which suggest that the first step in the formation of the MnZn ferrites was the precipitation of the zinc ferrite. The increase in the lattice parameter would reflect the inclusion of the manganese ion on the octahedral sites of the spinel lattice. In the present work, the lattice parameter evolution indicates that this Mn^{2+} inclusion was more effective at temperatures higher than 125 °C (Table 1). The values of the lattice parameter measured in the sintered samples are higher than that of the hydrothermal ferrite powders. Since there are no compositional differences between the powders and the sintered materials, the lattice parameter variations can be attributed to the inclusion of manganese ions in the octahedral sites of the spinel also during sintering.

It is well known that the magnetic properties of sintered ferrites are greatly influenced by the oxygen partial pressure exerted during sintering.[15] This is particularly true for manganese ferrites, since manganese is able to acquire different valences during sintering. The interchange of the ions by diffusion occurs on the surface of the sample. The sintering atmosphere must be such that no reception or delivery of gas or metal ions is possible. The first step in controlling these reactions is the nitrogen sintering of MnZn ferrites. It is necessary to supervise first of all the zinc volatilisation from surface and also the amount of oxygen in the bulk of the sample. The vapour pressure of zinc oxide is substantially higher than that of the other metal ions. By careful handling during production, using pure reagents and by adjusting sintering methods which keep zinc volatilisation to a minimum, the final properties can be optimised.[13]

The results showed in Fig. 7 indicated that when a low-oxygen content sintering atmosphere was used, either grain boundary velocity was enhanced or pore velocity was suppressed. The oxygen pressure affects the cation vacancy concentration,[18] which governs the lattice diffusion during sintering of ferrites. An increase in the oxygen partial pressure leads to an increase in vacancy concentration and, consequently, in the grain growth kinetics.[18] Analysing the results of the present work, it can be inferred that the low oxygen concentration used reduces the vacancy flux along the boundary region, which increases the boundary velocity. Thus, the boundary detaches itself from pores which end up being trapped inside the grain. In the case of a pore, its migration occurs by diffusion on the pore surface or by transport of vapour across the pore.[19,20] At the pore region, oxygen is transported *via* the vapour phase and hence high oxygen vacancies do not affect the oxygen flux. However, the low cation vacancies can reduce the flux of cation diffusion and hence pore migration will be retarded. As a consequence, we observe numerous pores trapped inside the grains (Fig. 7). Majima *et al.*[14,15] and Drofenik *et al.*[21] suggested that when low zinc oxide loss occurred, it might enhance the grain boundary migration, resulting in the formation of giant grains. This was not observed in the present work, which shows that zinc volatilisation, if it occurred, could be neglected.

The magnetic character of the MnZn ferrites will be discussed now. It is well known that nanosized manganese zinc ferrite powders exhibit superparamagnetic character.[22] Large grain size ferrite ceramics exhibit a complex domain structure. When the size of the grains is reduced, the number of domains decreases, and a transition from a polydomain to a single domain structure occurs. At a still smaller grain size, the ferrite

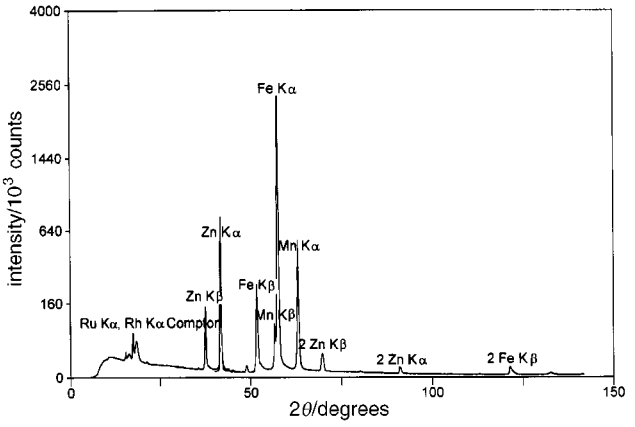

Fig. 8 XRF spectrum of the MnZn ferrite powder obtained at 110 °C

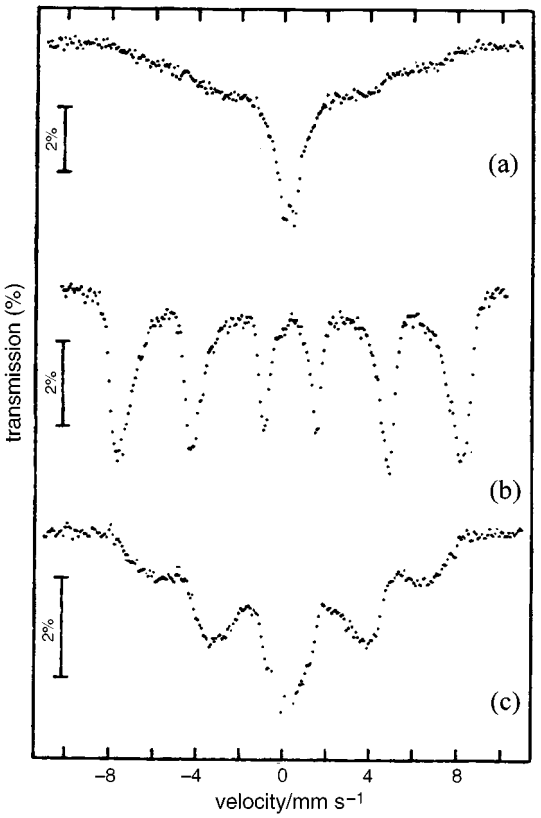

Fig. 9 Mössbauer spectra for the MnZn ferrite powder analysed (a) at room temperature, (b) at 77 K and (c) at 300 K with an applied magnetic field of 2 kG

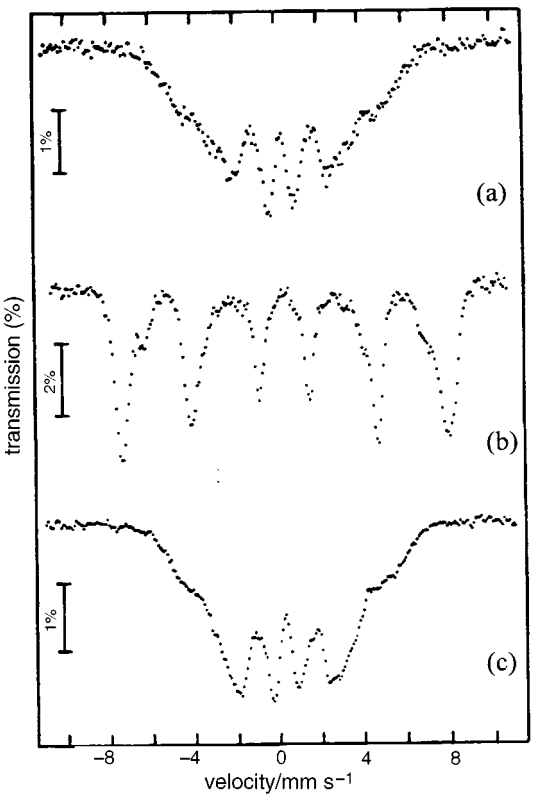

Fig. 10 Mössbauer spectra for the sintered bodies analysed (a) at room temperature, (b) at 77 K and (c) at 300 K with an applied magnetic field of 2 kG

particles undergo a phase change to a superparamagnetic solid. These particles may show a type of magnetic Brownian movement and tend to behave similar to a paramagnetic atom with a very large magnetic moment. In this work, the ferrite powders hydrothermally produced present particle sizes <30 nm, and thus exhibited a single quadrupole-split doublet in the Mössbauer spectrum at room temperature [Fig. 9(a)], which characterises the superparamagnetic behaviour. Below a certain temperature and/or above a certain particle volume, the relaxation time is long compared to the nuclear Larmor precession period,[23] and a magnetically split six-line pattern is obtained at 77 K [Fig. 9(b)]. When a magnetic field is applied to the superparamagnetic powder, the ferrimagnetic character can be evidenced [Fig. 9(c)]. During sintering, the particles grow and Mössbauer spectroscopy revealed, for the sintered ceramics, that the ferrites are ferrimagnetic in nature [Fig. 10(a)]. Fig. 10(b) and 10(c) illustrate the effect of the low-temperature analysis and of the applied magnetic field (at room temperature) on the magnetic behaviour of these materials. The above observations indicate that at 77 K the paramagnetic component is completely transformed into the ordered magnetic structure because the long-range magnetic interactions surmount the localised paramagnetic interactions.[24]

Conclusions

High quality MnZn ferrites can be produced from hydrothermally processed oxide powders. The analysis of the morphological characteristics of MnZn ferrites showed that the changes in lattice parameter, particle size, density, size and total volume of pores and in the surface area of the particles are functions of the hydrothermal temperature and time. The results presented in this work show that the sintering of submicrometer-sized hydrothermally processed MnZn ferrite powders leads to high density and surface homogeneous ceramic bodies. The sintering atmosphere was adequate, since no zinc volatilisation occurred. The lattice parameter variations were a consequence of changes in the cation distributions; in particular, manganese ions were introduced in the octahedral sites of the spinel during the sintering process.

Small differences observed on the properties of the synthesised powders lead to rather different microstructures after sintering. Specimens obtained from powders produced at higher temperatures have larger grains and less porosity. This behaviour was explained on the basis of the surface chemistry of the nanosized ferrite particles. As synthesis temperature increases, the number of water molecules and hydroxy groups on the particle surface decreases, enhancing the reactivity during the sintering process. Also, the sintering atmosphere used could be related to the final microstructure observed. The low oxygen content enhances the grain boundary migration (or reduces the pore velocity), leading to the detachment of the boundary from pores and to the appearance of intragranular porosity.

The results from Mössbauer spectroscopy showed that the MnZn ferrite powders were superparamagnetic in nature. The ferrimagnetic character of the MnZn ferrites produced hydrothermally are observed at room temperature with an applied magnetic field, at 77 K and after sintering. Under these conditions, an ordered magnetic structure was observed since the long-range magnetic interaction surmounts the localised paramagnetic interactions.

The authors thank the financial support from FAPEMIG.

References

1 H. Toraya, M. Yoshimura and S. Somiya, *J. Am. Ceram. Soc.*, 1982, **65**, C72.
2 S. Hirano, M. G. M. U. Ismail and S. Somiya, *J. Am. Ceram. Soc.*, 1976, **59**, 277.
3 S. Hirano, M. Ozawa and S. Naka, *J. Mater. Sci.*, 1981, **16**, 1989.
4 E. D. Kolb, R. L. Barns, R. A. Laudise and J. C. Grenier, *J. Cryst. Growth*, 1980, **50**, 404.
5 D. Louër, M. T. Mesnier and J. C. Niepce, *J. Mater. Sci.*, 1984, **19**, 716.
6 S. Lowell and J. E. Shields, *Powder Surface Area and Porosity*, Chapmann & Hall Ltd., New York, NY, 1987.
7 A. Dias, V. T. L. Buono, J. M. C. Vilela, M.S. Andrade and T. M. Lima, *J. Mater. Sci.*, 1997, **32**, 4715.
8 S. Komarneni, E. Fregeau, E. Breval and R. Roy, *J. Am. Ceram. Soc.*, 1988, **71**, C26.
9 A. Dias, R. L. Moreira and N. D. S. Mohallem, *J. Phys. Chem. Solids*, 1997, **58**, 543.
10 J. Zhao and M. P. Harmer, *J. Am. Ceram. Soc.*, 1988, **71**, 113.
11 J. Zhao and M. P. Harmer, *J. Am. Ceram. Soc.*, 1992, **75**, 830.
12 M. J. Readey, R. R. Lee, J. W. Halloran and A. H. Heuer, *J. Am. Ceram. Soc.*, 1990, **73**, 1499.
13 P. Sainanthip and V. R. W. Amarakoon, *J. Am. Ceram. Soc.*, 1988, **71**, 644.
14 K. Majima, M. Hasegawa, S. Katsuyama, H. Nagai and S. Mishima, *J. Mater. Sci. Lett.*, 1993, **12**, 185.
15 K. Majima, M. Hasegawa, M. Yokota, H. Nagai and S. Mishima, *Mater. Trans. JIM*, 1993, **34**, 556.
16 M. Zaharescu, M. Balasoni, M. Crisan, D. Crisan, T. Tavala and V. Moser, *Rev. Roum. Chim.*, 1984, **29**, 247.
17 O. Kimura and A. Chiba, *Adv. Ceram.*, 1986, **15**, 115.
18 H. Rikukawa and I. Sasaki, *Adv. Ceram.*, 1986, **15**, 215.
19 J. Svoboda and H. Riedel, *Acta Metall. Mater.*, 1992, **40**, 2829.
20 J. Svoboda and H. Riedel. *Acta Metall. Mater.*, 1993, **41**, 1929.
21 M. Drofenik and S. Besenicar, *Am. Ceram. Soc. Bull.*, 1986, **65**, 656.
22 T. Pannaparayil, R. Marande and S. Komarneni, *J. Appl. Phys.*, 1991, **69**, 5349.
23 W. Kündig, H. Bömmel, G. Constabaris and H. Lindquist, *Phys. Rev,*, 1966, **142**, 327.
24 H. H. Joshi, P. B. Pandya and R. G. Kulkarni, *Solid State Comm.*, 1993, **86**, 807.

Paper 7/04032F; *Received* 10*th June*, 1997